

THE 2009 DECEMBER GAMMA-RAY FLARE OF 3C 454.3: THE MULTIFREQUENCY CAMPAIGN

L. PACCIANI¹, V. VITTORINI^{1,2}, M. TAVANI^{1,2}, M. T. FIOCCHI¹, S. VERCELLONE³, F. D'AMMANDO³, T. SAKAMOTO^{4,5,6}, E. PIAN^{7,8}, C. M. RAITERI⁹, M. VILLATA⁹, M. SASADA¹⁰, R. ITOH¹⁰, M. YAMANAKA^{10,11}, M. UEMURA¹¹, E. STRIANI^{2,12}, D. FUGAZZA¹³, A. TIENGO¹⁴, H. A. KRIMM^{4,6,15}, M. C. STROH¹⁶, A. D. FALCONE¹⁶, P. A. CURRAN¹⁷, A. C. SADUN¹⁸, A. LAHTENMAKI¹⁹, M. TORNIKOSKI¹⁹, H. D. ALLER²⁰, M. F. ALLER²⁰, C. S. LIN²¹, V. M. LARIONOV^{22,23,24}, P. LETO²⁵, L. O. TAKALO²⁶, A. BERDYUGIN²⁶, M. A. GURWELL²⁷, A. BULGARELLI²⁸, A. W. CHEN^{14,29}, I. DONNARUMMA¹, A. GIULIANI¹⁴, F. LONGO³⁰, G. PUCELLA³¹, A. ARGAN¹, G. BARBIELLINI³⁰, P. CARAVEO¹⁴, P. W. CATTANEO³², E. COSTA¹, G. DE PARIS¹, E. DEL MONTE¹, G. DI COCCO²⁸, Y. EVANGELISTA¹, A. FERRARI³³, M. FEROCI¹, M. FIORINI¹⁴, F. FUSCHINO²⁸, M. GALLI³⁴, F. GIANOTTI²⁸, C. LABANTI²⁸, I. LAPSHOV¹, F. LAZZAROTTO¹, P. LIPARI³⁵, M. MARISALDI²⁸, S. MEREGHETTI¹⁴, E. MORELLI²⁸, E. MORETTI³⁰, A. MORSELLI¹², A. PELLIZZONI³⁶, F. PEROTTI¹⁴, G. PIANO^{1,2,12}, P. PICOZZA^{2,12}, M. PILIA^{37,36}, M. PREST³⁷, M. RAPISARDA³¹, A. RAPPOLDI³², A. RUBINI¹, S. SABATINI¹, P. SOFFITTA¹, M. TRIFOGLIO²⁸, A. TROIS¹, E. VALLAZZA³⁰, D. ZANELLO³⁵, S. COLAFRANCESCO³⁸, C. PITTORI³⁸, F. VERRECCHIA³⁸, P. SANTOLAMAZZA³⁸, F. LUCARELLI³⁸, P. GIOMMI³⁸, AND L. SALOTTI³⁹

¹ INAF/IASF-Roma, I-00133 Roma, Italy; luigi.pacciani@iasf-roma.inaf.it

² Dip. di Fisica, Univ. Tor Vergata, I-00133 Roma, Italy

³ INAF-IASF Palermo, Via Ugo La Malfa 153, I-90146 Palermo, Italy

⁴ Center for Research and Exploration in Space Science and Technology (CRESTT), NASA Goddard Space Flight Center, Greenbelt, MD 20771, USA

⁵ Joint Center for Astrophysics, University of Maryland, Baltimore County, 1000 Hilltop Circle, Baltimore, MD 21250, USA

⁶ NASA Goddard Space Flight Center, Greenbelt, MD 20771, USA

⁷ INAF-OATS, Via Tiepolo 11, I-34143 Trieste, Italy

⁸ SNS, Piazza dei Cavalieri, 7, I-56126 Pisa, Italy

⁹ OATO-INAf, Strada Osservatorio 20, I-10025, Pino Torinese (To), Italy

¹⁰ Department of Physical Science, Hiroshima University, Kagamiyama 1-3-1, Higashi-Hiroshima 739-8526, Japan

¹¹ Hiroshima Astrophysical Science Center, Hiroshima University, Kagamiyama 1-3-1, Higashi-Hiroshima 739-8526, Japan

¹² INFN Roma Tor Vergata, I-00133 Roma, Italy

¹³ OAB-INAf, via Brera 28, I-20121 Milano, Italy

¹⁴ INAF/IASF-Milano, I-20133 Milano, Italy

¹⁵ Universities Space Research Association, 10211 Wincopin Circle, Suite 500, Columbia, MD 21044-3432, USA

¹⁶ Department of Astronomy and Astrophysics, Pennsylvania State University, University Park, PA 16802, USA

¹⁷ Mullard Space Science Laboratory, University College London, Holmbury St. Mary, Dorking, RH5 6NT, UK

¹⁸ University of Colorado, Denver, USA

¹⁹ Aalto University Metsähovi Radio Observatory, Metsahovintie 114, FIN-02540 Kylmala, Finland

²⁰ Department of Astronomy, University of Michigan, USA

²¹ Institute of Astronomy, National Central University, Chung-Li, Taiwan 32054, China

²² Astronomical Institute, Saint-Petersburg State University, Russia

²³ Pulkovo Observatory, Saint-Petersburg, Russia

²⁴ Isaac Newton Institute of Chile, Saint-Petersburg Branch, Russia

²⁵ INAF, Osservatorio Astrofisico di Catania, Italy

²⁶ Tuorla Observatory, Department of Physics and Astronomy, University of Turku, FI-21500 Piikkiö, Finland

²⁷ Harvard-Smithsonian Center for Astrophysics, Cambridge, MA, USA

²⁸ INAF/IASF-Bologna, I-40129 Bologna, Italy

²⁹ CIFS-Torino, I-10133 Torino, Italy

³⁰ Dip. Fisica and INFN Trieste, I-34127 Trieste, Italy

³¹ ENEA Frascati, I-00044 Frascati (Roma), Italy

³² INFN-Pavia, I-27100 Pavia, Italy

³³ Dip. Fisica, Università di Torino, Torino, Italy

³⁴ ENEA-Bologna, I-40129 Bologna, Italy

³⁵ INFN-Roma La Sapienza, I-00185 Roma, Italy

³⁶ INAF-OAC, localita' Poggio dei Pini, strada 54, I-09012 Capoterra, Italy

³⁷ Dip. di Fisica, Univ. Dell'Insubria, Via Valleggio 11, I-22100 Como, Italy

³⁸ ASI Science Data Center, I-00044 Frascati (Roma), Italy

³⁹ Agenzia Spaziale Italiana, I-00198 Roma, Italy

Received 2010 April 15; accepted 2010 May 17; published 2010 June 2

ABSTRACT

During the month of 2009 December, the blazar 3C 454.3 became the brightest gamma-ray source in the sky, reaching a peak flux $F \sim 2000 \times 10^{-8}$ photons $\text{cm}^{-2} \text{s}^{-1}$ for $E > 100$ MeV. Starting in 2009 November intensive multifrequency campaigns monitored the 3C 454 gamma-ray outburst. Here, we report on the results of a two-month campaign involving *AGILE*, *INTEGRAL*, *Swift*/XRT, *Swift*/BAT, and *Rossi XTE* for the high-energy observations and *Swift*/UVOT, KANATA, Goddard Robotic Telescope, and REM for the near-IR/optical/UV data. GASP/WEAT provided radio and additional optical data. We detected a long-term active emission phase lasting ~ 1 month at all wavelengths: in the gamma-ray band, peak emission was reached on 2009 December 2–3. Remarkably, this gamma-ray super-flare was not accompanied by correspondingly intense emission in the optical/UV band that reached a level substantially lower than the previous observations in 2007–2008. The lack of strong simultaneous optical brightening during the super-flare and the determination of the broadband spectral evolution severely constrain the theoretical modeling. We find that the pre- and post-flare broadband behavior can be explained by a one-zone model involving synchrotron self-Compton plus external Compton emission from an

accretion disk and a broad-line region. However, the spectra of the 2009 December 2–3 super-flare and of the secondary peak emission on 2009 December 9 cannot be satisfactorily modeled by a simple one-zone model. An additional particle component is most likely active during these states.

Key words: galaxies: active – galaxies: individual (3C 454.3) – quasars: general – radiation mechanisms: non-thermal

1. INTRODUCTION

The flat spectrum radio quasar 3C 454.3 (at a redshift $z = 0.859$) turns out to be among the most active blazars emitting a broad spectrum ranging from radio to gamma-ray energies. Blazars are a sub-class of active galactic nuclei, with the relativistic jet aligned to the line of sight. Their spectral energy distributions (SEDs) typically show a double humped shape, with the low-energy peak lying between radio and X-rays and the high-energy peak in the GeV–TeV band (Urry & Padovani 1995). A detailed description of blazar leptonic emission models can be found in Maraschi et al. (1992), Marscher & Bloom (1992) and Sikora et al. (1994). The observed spectra can also be modeled in the framework of hadronic models (Mucke and Protheroe 2001; Mucke et al. 2003; Bottcher 2007).

Starting in 2004–2005, 3C 454.3 showed a long period of optical activity, with variability timescale ranging from several months to less than one day. In 2005 May, the source reached a peak magnitude $R \simeq 12$ showing strong 1 day variability (Villata et al. 2006). A radio peak was detected nine months after the optical peak, with fluxes of 22 Jy at 37 GHz and 20 Jy at 43 GHz (Villata et al. 2007). The source was then quiescent from the beginning of 2006 until mid-2007 (with an R magnitude between 15 and 16; Raiteri et al. 2008). Starting in the second half of 2007 (Vercellone et al. 2008), 3C 454.3 has been detected in a high gamma-ray state by *AGILE* (Tavani et al. 2009) and, subsequently, also by *Fermi Large Area Telescope* (Atwood et al. 2009; Abdo et al. 2009). Typically, the level of gamma-ray activity (with a flux of $(300\text{--}600) \times 10^{-8}$ photons $\text{cm}^{-2} \text{s}^{-1}$ for $E > 100$ MeV) has been observed to be correlated with the optical emission. Relatively large gamma-ray fluxes were detected during the *AGILE* observations of 2007 (Vercellone et al. 2008, 2009a; Donnarumma et al. 2009). During 2008, the source that was bright at the beginning of the year, started to fade in the optical band (Villata et al. 2009). *AGILE* detected the fading in gamma rays too (Vercellone et al. 2010). *Fermi* reported an averaged spectrum above 200 MeV with a photon index $\alpha \simeq 2.3$ and a spectral break at $E_c \sim 2.4$ GeV, obtained in 2008 August (Abdo et al. 2009).

2. THE MULTIFREQUENCY CAMPAIGN

The intensive monitoring of 3C 454.3 carried out by our group covered the period of extraordinary gamma-ray activity in 2009 November–December (Striani et al. 2009a, 2009b). The campaign involved *AGILE* for the gamma-ray band, *Swift*/Burst Alert Telescope (BAT), *Rossi XTE*/HEXTE, and *INTEGRAL*/IBIS in the hard X-ray band, *Rossi XTE*/PCA and *Swift*/XRT in X-rays, *Swift*/UVOT in the optical and UV bands, the KANATA observatory and Goddard Robotic Telescope (GRT) in the optical, and Rapid Eye Mount (REM; Zerbi et al. 2001) in the near infrared and optical. *AGILE* observed the source every day in spinning mode, scanning about 70% of the whole sky every 6 minutes. *International Gamma-Ray Astrophysics Laboratory* (*INTEGRAL*) pointed the source in response to a Target of Opportunity (ToO) observations (Vercellone et al.

2009b) and observed it from 2009 December 6 until 2009 December 12. The *Rossi XTE* satellite observed 3C 454.3 on 2009 December 5 and then daily from 2009 December 8 until 2009 December 17 for typical integrations of ~ 3 ks. *Swift* started to observe 3C 454.3 on 2009 November 27, in response to a ToO, and pointed at the source every day (UVOT performed most of the observations with UV filters). The KANATA 1.5 m telescope performed a long source monitoring in the V band with a time step of 1 day. The fully automated 14" GRT performed observations in the V and R bands, quasi-simultaneously with *Swift*, starting on 2009 November 30. REM started the 3C 454.3 monitoring on 2009 December 10 in response to a ToO and observed the source every day in the *VRJHK* filters. The *GLAST-AGILE* Support Program (GASP; Villata et al. 2008, 2009) performed an intensive monitoring campaign of the source in 2009–2010. We used a sub-sample of their data: optical observations reported in this Letter were performed at Lulin, New Mexico Skies, Roque de los Muchachos (KVA), and Saint Petersburg. GASP radio data were taken at Mauna Kea (The Submillimeter Array (SMA), 230 GHz), Noto (43 GHz), Metsähovi (37 GHz), and UMRAO (4.8, 8.0, and 14.5 GHz).

3. DATA ANALYSIS

AGILE/GRID data were analyzed using the Build-19 software and the response matrix v10 calibrated in the energy range 100–3000 MeV. Well-reconstructed gamma-ray events were selected using the FM3.119 filter. All the events collected during the passage in the South-Atlantic Anomaly were rejected. We filtered out the Earth-albedo, rejecting photons coming from a circular region of radius 85° and centered on the Earth. We rejected photons with polar direction $> 35^\circ$ in the GRID reference system. Gamma-ray data were analyzed with integrations of 1 or 2 days, depending on the source flux. We used the standard *AGILE* Maximum-Likelihood procedure (ALIKE; see Mattox et al. 1996 for the concept definition) for each data set. The integration over 5 weeks from 2009 November 18 to 2009 December 23 UTC yields a photon index 1.88 ± 0.08 (all the errors reported in this Letter are at 1σ , except where stated).

The *INTEGRAL*-IBIS (Ubertini et al. 2003) data were processed using the OSA software version 8.0. Light curves (from 20 to 200 keV) and spectra (from 18 to 200 keV) were extracted for each individual science window of revolutions 873 and 874.

The *Swift*-BAT survey data were obtained applying the “BAT FOV” option. The data have been processed by *batsurvey* script available through HEASOFT software package with a snapshot (single pointing) interval. To estimate the background, 10 background points around the source in a radius of $50'$ are selected. The source, 10 background points, and the bright hard X-ray sources (for cleaning purpose) are included in the input catalog of *batsurvey*. The BAT count rate in the 14–195 keV band has been converted into the energy flux assuming a power-law photon index 1.7 as determined from the *INTEGRAL*-ISGRI data, see below. In order to match with the HEXTE range, the BAT hard X-ray flux has been rescaled in Figure 1 to the 20–40 keV band.

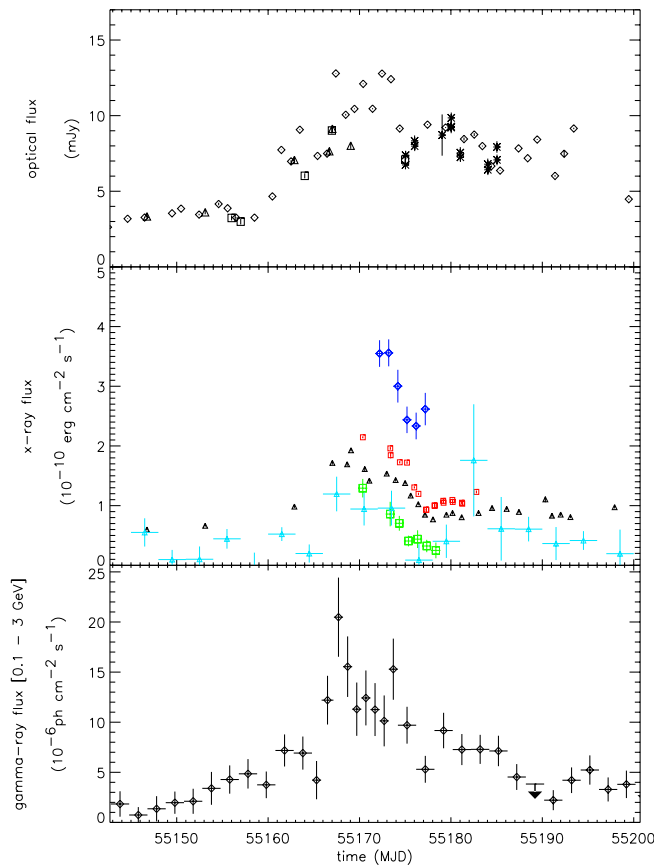


Figure 1. Multifrequency data collected during the campaign. Upper panel: optical V data from: KANATA (diamonds), REM (star), GRT (squares), UVOT (triangles). Middle panel: X-ray data from XRT (0.3–10 keV flux, black triangles), PCA (3–20 keV, red squares), HEXTE (20–40 keV, green squares), BAT (14–195 keV rate, rescaled to the 20–40 keV band, cyan triangles), ISGRI (20–200 keV, blue diamonds). Bottom panel: gamma-ray data from the *AGILE*-GRID (0.1–3 GeV, black diamonds).

Rossi XTE-PCA (Jahoda et al. 1996) and HEXTE (Rothschild et al. 1998) data were analyzed following the same procedure as described in Vercellone et al. (2010). The data analysis was restricted to the PCU2 in the 3–20 keV energy range for the Proportional Counter Array (PCA) and to the Cluster B in the 18–50 keV range for the HEXTE. The net exposure times were 27.3 ks for PCA and 7.3 ks for HEXTE. The background-subtracted source spectra obtained with both the instruments were simultaneously fit⁴⁰ with an absorbed power-law model, with the photoelectric absorption fixed to $0.134 \times 10^{22} \text{ cm}^{-2}$ (Villata et al. 2006). After the introduction of a 2% systematic error, the best-fit value for the photon index is 1.74 ± 0.01 .

The *Swift*-XRT data were processed using the most recent calibration files available. We utilized *Swift* Software version 3.5, FTOOLS version 6.8, and XSPEC version 12.5.1n. We fitted the data with an absorbed power-law model. We obtained photon indices between 1.51 ± 0.09 and 1.73 ± 0.11 and excess absorption between $(0.09 \pm 0.06) \times 10^{22}$ and $(0.17 \pm 0.03) \times 10^{22} \text{ cm}^{-2}$ (all uncertainties on XRT spectral fit are at the 90% level).

Swift-UVOT data from each observation sequence were processed by the standard UVOT tool `uvotsource` using the

same version of the *Swift* software as for the XRT analysis. An extraction region of radius 5 arcsec centered on the source and a suitable background region were used. Magnitudes are based on the UVOT photometric system (Poole et al. 2008).

The optical photometry of the Kanata Observatory data was performed using TRISPEC (Watanabe et al. 2005). The observations were pipeline-reduced, including bias removal and flat-field corrections. We derived the V-band magnitude from differential photometry with a nearby reference star, USNOB 1061-0614254 (see Gonzales-Perez et al. 2001). Photometric stability of this star has been confirmed by our simultaneous photometry for another nearby star, USNOB 1061-0614207.

All REM raw optical and NIR frames, obtained with ROSS (Tosti et al. 2004) and REMIR (Conconi et al. 2004), respectively, as well as images from GRT were corrected for dark, bias, and flat field following standard recipes. Instrumental magnitudes were obtained via aperture photometry, and absolute calibration has been performed by means of secondary standard stars in the field (Raiteri et al. 1998).

Even if it is not shown in Figure 1, the Metsähovi radio data at 37 GHz show a high flux with an increasing trend from 2009 December 1 until 2010 January 14 and a mean flux of ~ 20 Jy during the first week of 2009 December. The mean 230 GHz flux is ~ 25 Jy. These radio fluxes⁴¹ are comparable to the peak flux measured in 2006 (Villata et al. 2007).

All UV/optical/NIR data presented here were corrected for the Galactic extinction toward 3C 454.3 assuming $A_V = 0.349$ (Schlegel et al. 1998).

4. RESULTS

The multifrequency light curves of 3C 454.3 are shown in Figure 1. The exceptional gamma-ray flaring activity is produced during an extended period lasting several weeks. The broadband coverage is excellent, and for the first time allows a detailed multiwavelength study of a gamma-ray blazar peaking above the Vela pulsar flux (for comparison, see the multifrequency coverage for the gamma-ray super-flare of PKS 1622-29; Mattox et al. 1997).

The optical data show variability timescale as short as 1 day or less. Due to a typical interval between optical observations (1 day), we did not show in Figure 1 a detailed representation of the variability. The optical V data indicate a low state of the source ($V > 15$ mag, flux < 3.9 mJy) until MJD 55160, after which the flux started to increase. The optical flux increased about 50% in less than 1 day from MJD 55166.4 until MJD 55167.4, reaching the value $V = 13.7$ mag (e.g., 12.8 mJy), followed by a fast flux decrease to $V = 14.3$ mag (e.g., 7.4 mJy) at MJD 55169.0. Another optical peak was reached at MJD 55172.5 ($V = 13.7$ mag), and was then followed by a minimum at MJD 55175.0, with $V = 14.4$ mag (e.g., 6.7 mJy).

In general, the X-ray flux follows⁴² the rising part of the optical emission in the interval MJD 55150–55169. Starting on MJD 55169, the X-ray flux started to fade, with the optical emission remaining in a relatively high state for 4–5 days. Our *INTEGRAL* hard X-ray data sample the fading phase of the high-activity period.

We performed a discrete correlation function analysis for the optical–gamma and soft X–gamma data set. No significant

⁴⁰ The resulting fit is not statistically acceptable ($\chi_{\text{red}}^2 = 1.53/54$ dof); however, the addition of a 2% systematic error to the data, which is well within the expected uncertainties in the spectral calibration, is sufficient to make the fit fully acceptable ($\chi_{\text{red}}^2 = 1.02/54$ dof).

⁴¹ The long-term radio and optical light curves of 3C 454.3 during the 2009–2010 observing season will be presented in a forthcoming paper (C. M. Raiteri et al. 2010, in preparation).

⁴² We note that no X-ray data were obtained in exact correspondence with the gamma-ray super-flare of 2009 December 2–3.

delay is found within 2 days (compatible with the average bin of gamma-ray light curve).

We focused on the time-dependent spectral analysis of this exceptional activity of 3C 454.3 and used simultaneous broadband data to obtain a detailed account of the source variability. We obtained the SED for four periods. The first period (interval-1) is for a 5 day integration of GRID data, centered at 2009 November 27 09:36 UT (MJD 55162.4), and using the *Swift* observation at MJD 55162.9, and quasi-simultaneous GASP optical data (from KVA and New Mexico Skies) obtained within 16 hr from the *Swift* observation (pre-flare SED).

The second period (interval-2) was obtained for the gamma-ray super-flare episode integrating the GRID data for 1 day centered at 2009 December 2 16:48 UT (MJD 55167.7) and using the simultaneous *Swift* and GRT observations at MJD 55167.0 (first flare SED). The Kanata observatory measured a flux 40% higher in the V band 10 hr after the GRT observation.

The third SED was obtained (interval-3) integrating GRID data for 2 days centered at 2009 December 6 16:48 UT (MJD 55172.7), to match the local maximum of the optical light curve with $V = 13.7$ mag that is apparently coincident with the secondary gamma-ray maximum near MJD 55174. For this interval, we used the *INTEGRAL*-ISGRI data collected between MJD 55171.7 and MJD 55174.2, *Swift* data at MJD 55173.9, *Rossi XTE* data at 55173.4, and GASP optical data (from Lulin and GRT) obtained within 26 hr from the *Swift* data.

The last SED (interval-4) was obtained integrating GRID data for 5.5 days centered at 2009 December 15 18:00 UT (MJD 55180.8) and making use of the *Swift* observation at MJD 55179.1, the *Rossi XTE* observation at MJD 55179.2, the GASP optical data (from Saint Petersburg and Lulin) simultaneous with *Swift* within 12 hr, and the near-infrared observations from REM at MJD 55181.0 (post-flare SED).

Radio data for the SEDs were taken by the GASP, using observations from Mauna Kea (SMA, 230 GHz), Noto (43 GHz), Metsähovi (37 GHz), UMRAO (4.8, 8.0, 14.5 GHz), and simultaneous within a few days with the XRT observations. Due to the slow variability of the radio data, we use interpolated radio values in the SEDs. The results are shown in Figure 2.

5. DISCUSSION

The multifrequency data of the extensive campaign on 3C 454.3 show a remarkable behavior of the source. Starting from MJD 55150, first an overall rise of the gamma-ray emission is detected and then that of the X-ray and optical fluxes. This rise culminates with peak optical/X-ray/gamma-ray emission during a 10 day period centered around MJD 55173. Subsequently, the overall flux decreased and reached again a relative-minimum state around MJD 55200. During the two-month period, the optical and X-ray fluxes vary within a factor of 3, whereas the γ -ray flux grows by a factor of 5–10 compared to the pre-flare value. During the rapid super-flare around MJD 55167.7, the γ -ray flux doubles within 1 day with the optical and average X-ray increase of 50% and 30%, respectively.

We find an overall correlation at all wavelengths for both long and short timescales. However, the unusual gamma-ray flaring and super-flaring activity from 3C 454.3 during the period 2009 November–December is not accompanied by strong emission of similar intensity in the optical or even in the soft X-ray bands. The hard X-ray flux is comparable to the level of spring 2005, e.g., $\sim 3.5 \times 10^{-10}$ erg cm² s⁻¹ in 20–200 keV (Pian et al.

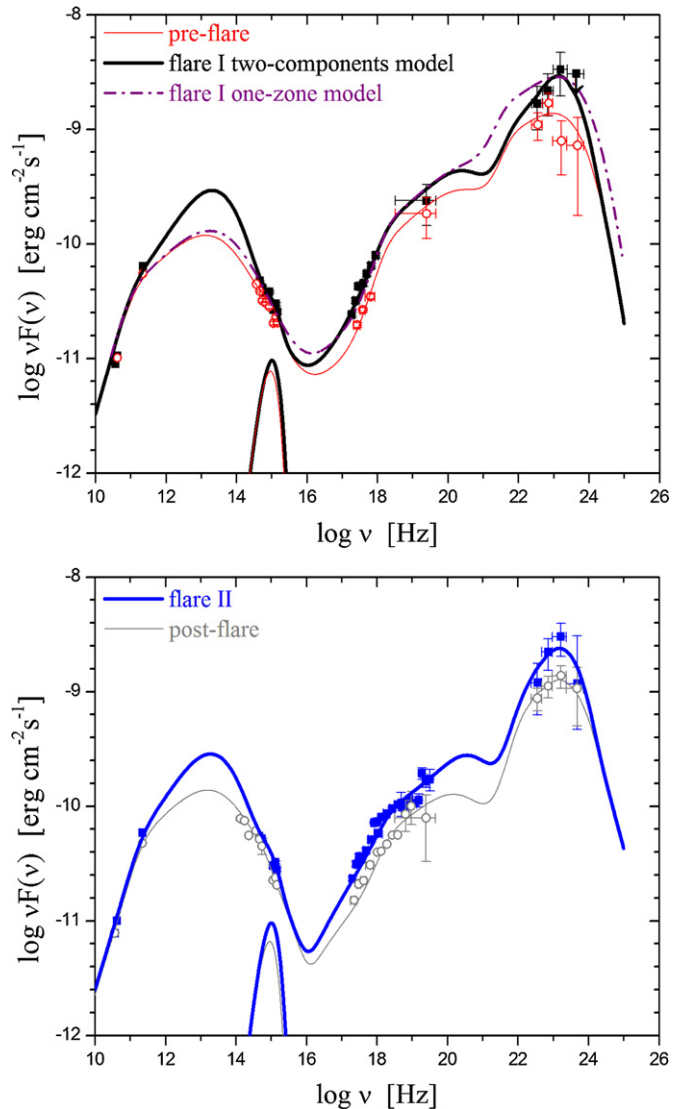


Figure 2. Multifrequency simultaneous spectra of 3C 454.3 at four different epochs superimposed with spectral modeling. Top panel: pre-flare (red open circles) and super-flare (black filled squares). Bottom panel: secondary flare (blue filled squares) and post-flare spectra (gray open circles). Models are detailed in the text.

2006). This flaring behavior appears to be quite different from other episodes detected in 2007 and 2008 (e.g., Vercellone et al. 2009a; Donnarumma et al. 2009). The synchrotron emission appears to be quite broad and centered around $\nu \sim 10^{13}$ Hz.

Striani et al. (2010) provided a first report of the *AGILE*-GRID data. A single power-law approximation gives a photon spectral index 1.66 ± 0.32 in the energy band 0.1–1 GeV, integrating the data for 2 days centered at MJD 55167.7. We confirm this result in the analysis presented here integrating gamma-ray data for 1 day, as shown in our Figure 2 (left panel). In addition, we found a similar spectral shape of the gamma-ray emission during the secondary maximum of interval-3. Our Figure 2 (right panel) shows the interval-3 SED as compared with the post-flare SED of interval-4.

The simultaneous observations of 3C 454.3 by *AGILE*, *INTEGRAL*, *Rossi XTE*, and *Swift* strongly constrain the emission models in the high-energy range. In particular, our interval-3 spectrum (blue solid squares of Figure 2, right panel) represents one of the best constrained multifrequency spectra ever obtained for a flaring blazar from X-ray up to GeV energies.

Table 1
Models Parameters Used for Producing the Spectral Analysis of Figure 2

Interval	Model	Component	B (G)	R (cm)	K (cm^{-3})	γ_b	γ_{\min}	ζ_1	ζ_2	Comments
1 (pre-flare)	Two component	Component-1 ^a	0.6	7×10^{16}	2.2	800	35	2.35	4.5	Broken PL
		Component-2
2 (super-flare)	Two component	Component-1	0.6	7×10^{16}	2.2	800	35	2.35	4.5	Broken PL
		Component-2	0.9	3×10^{16}	180	180	1	Relativistic Maxwellian
		One zone	0.5	7×10^{16}	2.5	1000	35	2.35	4.5	Broken PL
3 (secondary-flare)	Two component	Component-1	0.6	7×10^{16}	2.5	800	45	2.25	4.5	Broken PL
		Component-2	0.9	3×10^{16}	170	170	1	Relativistic Maxwellian
4 (post-flare)	Two component	Component-1 ^a	0.6	7×10^{16}	2.5	800	45	2.25	4.5	Broken PL
		Component-2

Notes. The columns give the emission interval specification, the leptonic component that dominates the gamma-ray emission, the magnetic field B , the comoving emission radius R , the particle energy distribution normalization K , the break energy (Lorentz factor) γ_b , the minimum particle energy γ_{\min} , and the low- (ζ_1) and high-energy spectral indices (ζ_2) defined as $N(\gamma) = K \gamma_b^{-1} / [(\gamma/\gamma_b)^{\zeta_1} + (\gamma/\gamma_b)^{\zeta_2}]$. The relativistic Maxwellian is defined as $N(\gamma) = K (\gamma/\gamma_b) \exp(-\gamma/\gamma_b)$.

^a For the pre- and post-flare intervals, this set of parameters describes also the simple one-zone model.

We present in Figure 2 the results of our spectral modeling based on synchrotron self-Compton (SSC), plus contribution from external seed photons (EC). We used parameters similar to those already implemented to model previous gamma-ray flares of 3C 454.3. (Vercellone et al. 2009a; Donnarumma et al. 2009). We find that the pre- and post-flare spectra (interval-1 and interval-4) are adequately represented by a simple one-zone SSC model plus EC in which the accretion disk and the broad-line region provide the necessary soft radiation field for the inverse Compton components that dominate the X-ray through the GeV energies. The simple one-zone model parameters for the pre- and post-flare intervals are reported in Table 1 (they are also labeled component-1 in the table).

We can fit the super-flare with a simple one-zone model as shown in Figure 2 (dot-dashed curve), with the parameters reported in Table 1. Such a model requires (compared to the pre-flare fit parameters) an increase of the electron energy and density, and a slight reduction of the comoving magnetic field for the whole electron population of the blob (as also reported in Bonnoli et al. 2010). We note, however, that we used the optical data obtained during the rising edge of optical emission for the SED of the super-flare. Using only the V peak emission for the optical portion of the spectra, the one-zone model gives a magnetic field of 0.55 G, closer to the value for the pre-flare.

The time evolution of the source (e.g., the lack of strong optical emission and the gamma-ray spectrum during the super-flare) can also be described adopting a different approach. We assume a long-term rise and fall of the mass accretion rate onto the central black hole. This enhanced accretion causes an overall increase of the synchrotron emission and of the soft photon background scattered off by the primary component of accelerated electrons (component-1). An additional population of accelerated leptons (component-2, co-existing with component-1) can be introduced for the super-flare and secondary flare episodes. This component is a consequence of additional particle acceleration and/or plasmoid ejection near the jet basis. Table 1 reports the parameters that we used to model the Figure 2 spectra (the two-component models are shown as thick solid lines for the super-flare and for the secondary flare). For all intervals, we assume the presence of component-1. This is the only component acting for the pre- and post-flare intervals, with the parameters given in Table 1. The super-flare (secondary-flare) parameters

for component-1 are the same as the pre-flare (post-flare) interval. We assumed a bulk Lorentz factor $\Gamma = 25$, a jet angle with respect to the line of sight $\theta = 1^\circ.2$, and an accretion disk of bolometric luminosity $L_d = 6 \times 10^{46} \text{ erg s}^{-1}$ slowly decaying toward $L_d = 5 \times 10^{46} \text{ erg s}^{-1}$. A broad-line region located 0.5 pc from the black hole reflects 5% of the disk power toward the emitting regions.

The component-2 energy distribution that better reproduces our gamma-ray spectral data is a relativistic Maxwellian of characteristic energy $\gamma_b \simeq 180$. Interestingly, this component appears to be strongly energized but not yet modified by additional non-thermal acceleration.

This two-component approach avoids the problem of explaining the time variability of the physical parameters of the whole electron population of the one-zone model, at the price of adding an additional varying component superimposed with the pre-existing one.

To summarize, our multifrequency data for the 2009 December flare of 3C 454.3 provide a wealth of very important information on this puzzling and fascinating blazar. We find that 3C 454.3 is characterized by strong broadband spectral variability and that the modeling of the peak gamma-ray emission episodes suggests more elaborate models than the standard one-zone SSC+EC models of bright blazars.

The *AGILE* Mission is funded by the Italian Space Agency (ASI) with scientific and programmatic participation by the Italian Institute of Astrophysics (INAF) and the Italian Institute of Nuclear Physics (INFN). This investigation was carried out with partial support from the ASI contract no. I/089/06/2. V.L. acknowledges support from Russian RFBR foundation via grant 09-02-00092. The operation of UMRao is made possible by funding from the NSF, NASA, and the University of Michigan. The Submillimeter Array is funded by the Smithsonian Institution and the Academia Sinica Institute of Astronomy and Astrophysics. The GASP president acknowledges the ASI support through contract ASI-INAF I/088/06/0.

REFERENCES

- Abdo, A. A., et al. 2009, *ApJ*, 699, 817
Atwood, W. B., et al. 2009, *ApJ*, 697, 1071

- Bonnoli, G., et al. 2010, MNRAS, submitted (arXiv:1003.3476)
- Botcher, M. 2007, *Ap&SS*, 309, 95
- Conconi, P., et al. 2004, Proc. SPIE, 5492, 1602
- Donnarumma, I., et al. 2009, *ApJ*, 707, 1115
- Gonzalez-Perez, J. N., et al. 2001, *AJ*, 122, 2055
- Jahoda, K., et al. 1996, Proc. SPIE, 2808, 59
- Maraschi, L., Ghisellini, G., & Celotti, A. 1992, *ApJ*, 397, L5
- Marscher, A. P., & Bloom, S. D. 1992, Proc. Compton Observatory Science Workshop, ed. C. R. Schrader, N. Gehrels, & B. Dennis (Greenbelt, MD: NASA GSFC), 346
- Mattox, J. R., et al. 1996, *ApJ*, 461, 396
- Mattox, J. R., et al. 1997, *ApJ*, 476, 692
- Mucke, A., & Protheroe, R. J. 2001, *Astropart. Phys.*, 15, 121
- Mucke, A., et al. 2003, *Astropart. Phys.*, 18, 593
- Pian, E., et al. 2006, *A&A*, 449, L21
- Poole, T. S., et al. 2008, MNRAS, 383, 627
- Raiteri, C. M., et al. 1998, *A&A*, 130, 495
- Raiteri, C. M., et al. 2008, *A&A*, 491, 755
- Rothschild, R. E., et al. 1998, *ApJ*, 496, 538
- Schlegel, D. J., Finkbeiner, D. P., & Davis, M. 1998, *ApJ*, 500, 525
- Sikora, M., Begelman, M. C., & Rees, M. 1994, *ApJ*, 421, 153
- Striani, E., et al. 2009a, ATel, 2322
- Striani, E., et al. 2009b, ATel, 2326
- Striani, E., et al. 2010, ApJ, in press (arXiv:1005.4891)
- Tavani, M., et al. 2009, *A&A*, 502, 995
- Tosti, G., et al. 2004, Proc. SPIE, 5492, 689
- Ubertini, P., et al. 2003, *A&A*, 411, L131
- Urry, C. M., & Padovani, P. 1995, *PASP*, 107, 803
- Vercellone, S., et al. 2008, *ApJ*, 676, L13
- Vercellone, S., et al. 2009a, *ApJ*, 690, 1018
- Vercellone, S., et al. 2009b, ATel, 2344
- Vercellone, S., et al. 2010, *ApJ*, 712, 405
- Villata, M., et al. 2006, *A&A*, 453, 817
- Villata, M., et al. 2007, *A&A*, 464, L5
- Villata, M., et al. 2008, *A&A*, 481, L79
- Villata, M., et al. 2009, *A&A*, 504, L9
- Watanabe, M., et al. 2005, *PASP*, 117, 870
- Zerbi, R. M., et al. 2001, *Astron. Nachr.*, 322, 275